

In situ non-destructive measurement of Josephson junction resistance using fritting contact technique

Lei Du(杜磊), Hao-Ran Tao(陶浩然), Liang-Liang Guo(郭亮亮), Hai-Feng Zhang(张海峰), Yong Chen(陈勇), Xin Tian(田昕), Chi Zhang(张驰), Zhi-Long Jia(贾志龙), Peng Duan(段鹏), and Guo-Ping Guo(郭国平)

Citation: Chin. Phys. B, 2024, 33 (**11**): 110309. DOI: 10.1088/1674-1056/ad73b6
Journal homepage: http://cpb.iphy.ac.cn; http://iopscience.iop.org/cpb

What follows is a list of articles you may be interested in

Coupling and characterization of a Si/SiGe triple quantum dot array with a microwave resonator

Shun-Li Jiang(江顺利), Tian-Yi Jiang(蒋天翼), Yong-Qiang Xu(徐永强), Rui Wu(吴睿), Tian-Yue Hao(郝天岳), Shu-Kun Ye(叶澍坤), Ran-Ran Cai(蔡冉冉), Bao-Chuan Wang(王保传), Hai-Ou Li(李海欧), Gang Cao(曹刚), and Guo-Ping Guo(郭国平)

Chin. Phys. B, 2024, 33 (**9**): 090311. DOI: 10.1088/1674-1056/ad711d

In-situ deposited anti-aging TiN capping layer for Nb superconducting quantum circuits

Hao-Ran Tao(陶浩然), Lei Du(杜磊), Liang-Liang Guo(郭亮亮), Yong Chen(陈勇), Hai-Feng Zhang(张海峰), Xiao-Yan Yang(杨小燕), Guo-Liang Xu(徐国良), Chi Zhang(张 驰), Zhi-Long Jia(贾志龙), Peng Duan(段鹏), and Guo-Ping Guo(郭国平)

Chin. Phys. B, 2024, 33 (**9**): 090310. DOI: 10.1088/1674-1056/ad6a3c

A family of quantum von Neumann architecture

Dong-Sheng Wang(王东升)

Chin. Phys. B, 2024, 33 (**8**): 080302. DOI: 10.1088/1674-1056/ad50be

Electric field dependence of spin qubit in a Si-MOS quantum dot

Rong-Long Ma(马荣龙), Ming Ni(倪铭), Yu-Chen Zhou(周雨晨), Zhen-Zhen Kong(孔真真), Gui-Lei Wang(王桂磊), Di Liu(刘頔), Gang Luo(罗刚), Gang Cao(曹刚), Hai-Ou Li(李海欧), and Guo-Ping Guo(郭国平)

Chin. Phys. B, 2024, 33 (**6**): 060312. DOI: 10.1088/1674-1056/ad3812

Observation of the exceptional point in superconducting qubit with dissipation controlled by parametric modulation

Zhan Wang(王战), Zhongcheng Xiang(相忠诚), Tong Liu(刘桐), Xiaohui Song(宋小会), Pengtao Song(宋鹏涛), Xueyi Guo(郭学仪), Luhong Su(苏鹭红), He Zhang(张贺), Yanjing Du(杜燕京), and Dongning Zheng(郑东宁)

Chin. Phys. B, 2021, 30 (**10**): 100309. DOI: 10.1088/1674-1056/ac0520

SPECIAL TOPIC — Fabrication and manipulation of the second-generation quantum systems

In situ non-destructive measurement of Josephson junction resistance using fritting contact technique

Lei Du(杜磊)[1,2], Hao-Ran Tao(陶浩然)[1,2], Liang-Liang Guo(郭亮亮)[1,2], Hai-Feng Zhang(张海峰)[1,2], Yong Chen(陈勇)[1,2], Xin Tian(田昕)[3], Chi Zhang(张驰)[3], Zhi-Long Jia(贾志龙)[3], Peng Duan(段鹏)[1,2,†], and Guo-Ping Guo(郭国平)[1,2,3,‡]

[1] *CAS Key Laboratory of Quantum Information, University of Science and Technology of China, Hefei* 230026, *China*
[2] *CAS Center for Excellence and Synergetic Innovation Center in Quantum Information and Quantum Physics, University of Science and Technology of China, Hefei* 230026, *China*
[3] *Origin Quantum Computing Technology (Hefei) Co., Ltd., Hefei* 230088, *China*

(Received 22 July 2024; revised manuscript received 26 August 2024; accepted manuscript online 27 August 2024)

Conventional four-probe methods for measuring the resistance of Josephson junctions can damage superconducting thin films, making them unsuitable for frequency measurements of superconducting qubits. In this study, we present a custom probe station measurement system that employs the fritting contact technique to achieve *in situ*, non-destructive measurements of Josephson junction resistance. Our experimental results demonstrate that this method allows for accurate prediction of qubit frequency with an error margin of 17.2 MHz. Moreover, the fritting contact technique does not significantly affect qubit coherence time or the integrity of the superconducting film, confirming its non-destructive nature. This innovative approach provides a dependable foundation for frequency tuning and addressing frequency collision issues, thus supporting the advancement and practical deployment of superconducting quantum computing.

Keywords: non-destructive, fritting contact, qubit frequency, Josephson junction resistance

PACS: 03.67.Lx, 03.67.–a **DOI:** 10.1088/1674-1056/ad73b6

1. Introduction

Superconducting quantum computing has emerged as a promising approach for building scalable and fault-tolerant quantum computers.[1] The key component in superconducting qubits is the Josephson junction, which allows for the creation of quantum superposition and entanglement states essential for quantum computation.[2] However, as the number of qubits in a system increases, several challenges arise, including three-dimensional circuit integration,[3,4] readout fidelity,[5,6] and coherence time.[7,8] Among these challenges, frequency collisions stand out as a primary obstacle, directly impacting the selective control of qubits and the fidelity of two-qubit gates, particularly in fixed-frequency transmon structures.[9–12]

Frequency collisions occur due to fabrication errors in the chip manufacturing process, causing the frequencies of qubits to deviate from their design values.[13,15] These deviations lead to severe frequency collisions, necessitating measurement and assessment under cryogenic environments, which significantly consumes cryogenic resources and extends the testing cycle. Recently, post-processing techniques such as thermal annealing and laser annealing have shown excellent capabilities in tuning qubit frequencies,[16–18] making the prediction of qubit frequencies at room temperature essential for implementing these techniques.

In transmon qubits, the qubit frequency (f_q) is determined by the Josephson junction energy (E_J) and the charging energy (E_C), satisfying the relation $f_q \propto \sqrt{8E_J E_C}$.[19] The capacitance ($C_q$) of the qubit, typically taking the form of a coplanar waveguide capacitor, can be precisely fabricated. However, the critical current (I_c) of the Josephson junction, determined by its small area and barrier thickness, is susceptible to fabrication errors, which significantly contribute to qubit frequency deviations from the design value.[20–22] The relationship between I_c and the Josephson junction resistance (R_n) is given by the Ambegaokar–Baratoff relation $I_c = \frac{\pi\Delta}{2eR_n}$, where Δ is the superconducting energy gap. Therefore, by measuring R_n at room temperature, we can estimate f_q.

Conventional four-probe methods for measuring the resistance of Josephson junctions involve the probe scrubbing the film surface, mechanically penetrating the surface oxide layer and the film, and moving forward to establish a stable contact.[24] This method can leave micron-scale damage in the qubit capacitor area, potentially affecting the capacitor parameters and introducing impurities, which can become sources of decoherence.[18] Furthermore, commonly used superconducting films such as tantalum and niobium are relatively hard and not easily penetrated;[25,26] this leads to high contact resistance between the probe and the film, resulting in inaccurate measurements. Consequently, *in situ* R_n measurement using

†Corresponding author. E-mail: pengduan@ustc.edu.cn
‡Corresponding author. E-mail: gpguo@ustc.edu.cn

© 2024 Chinese Physical Society and IOP Publishing Ltd

traditional methods may lead to measurement inaccuracies and potential damage to the superconducting film.

To mitigate these issues, researchers often use non-*in situ* methods by preparing Josephson junction test structures at the edge of the superconducting chip to estimate f_q.[27–30] This approach involves fabricating additional test junctions with identical parameters on the periphery or non-critical regions of the chip. However, this method has significant limitations:

(i) Inability to detect random failures It cannot detect randomly failing qubits within the operational areas of the chip,[13] limiting the effectiveness of the measurements.

(ii) Dependence on fabrication uniformity The accuracy of frequency prediction is highly dependent on the uniformity of the fabrication process.[14] Any variations can lead to significant discrepancies between the test junctions and the actual operational junctions.

(iii) Localized nature of adjustments Techniques like laser annealing require precise knowledge of the actual resistance of the operational junctions to fine-tune the qubit frequencies effectively. The non-*in situ* nature of the test junction measurements does not provide this level of precision.

In this study, we address these limitations by utilizing the fritting contact technique to achieve *in situ*, non-destructive measurements of Josephson junction resistance. Fritting contact involves electrically breaking down the metal oxide layer by applying a controlled voltage, resulting in minimal physical damage to both the electrode and the probe while maintaining stable electrical contact. Our experimental results demonstrate that this method allows for accurate prediction of qubit frequency with an error margin of 17.2 MHz. Furthermore, we show that fritting contact does not significantly affect qubit coherence time or the integrity of superconducting film, confirming the non-destructive nature of this method. This advancement provides a significant technological foundation for frequency tuning and addressing frequency collision issues in multi-qubit systems, thereby accelerating the scalability and application of superconducting quantum computing.

2. Method

Fritting contact is a method used to achieve electrical contact by electrically breaking down the metal oxide layer. This method involves applying a low force to bring the probe into contact with the electrode and then applying a high voltage to the probe, inducing electron transition or ionization within the metal oxide layer to form a stable electrical contact. The advantage of this method lies in its minimal physical damage to both the electrode and the probe while maintaining the stability of the electrical contact.[31–33] To employ the fritting contact method, we built a custom probe station measurement system, as shown in Fig. 1(a). The chip is vacuum-adhered to a four-axis motorized stage. The probe, driven by a piezoelectric platform (P-611Z, PI), approaches the chip at a descent speed of 5 nm/s. The contact force between the probe and the chip is monitored in real-time using a micro-force sensor (μ-Force 20g, Chief SI) positioned between the stage and the probe, with a resolution of 5 μN. When the probe makes contact with the sample, the contact force starts to appear and increases to a preset value, at which point the stage stops moving, completing the contact process. This entire process is fully automated. The probe is made of tungsten, with a tip diameter of 200 nm. Imaging is performed using a CCD camera and a light source, with the microscope lens angled to ensure observation of the probe tip during the fritting contact process. The entire setup is placed on an active vibration isolation table to mitigate environmental noise, ensuring accurate contact force measurements.

Figure 1(b) illustrates the circuit used during the fritting contact and Josephson junction resistance measurement. First, after the probe contacts the qubit capacitor, a 20 ms pulse voltage signal is applied between contact points A and B, fritting the oxide layer. The pulse signal reduces circuit heating and minimizes damage to the film. Once electrical contact is established, the current limiter of the SMU is activated to prevent chip damage. The contact resistance is then measured. Electrical contact at points C and D is established using the same method. Finally, the SMU switch is turned off, and the circuit is switched to Josephson junction measurement circuit. Two lock-in amplifiers are used as an AC signal source and voltmeter for four-terminal measurements. The AC signal in the circuit eliminates the effects of thermoelectric and contact potentials that give rise to low-frequency noise. To protect Josephson junction, a 1 MΩ resistor is connected in series in the circuit to limit the current. The chip unit structure studied is shown in Fig. 1(b). The substrate is high resistivity ($>$ 10 kΩ·cm) intrinsic (100) plane silicon, and qubit is transmon structure formed by an aluminum coplanar waveguide capacitor and an Al/AlO_x/Al junction in parallel. The aluminum film is prepared by electron beam evaporation, and the Josephson junction is fabricated using the Manhattan-style technique, with an area of ~ 0.04 μm^2. Qubits are driven and read out through the readout bus.

3. Results and analysis

Fritting voltage and contact force are two critical parameters that determine the success rate of fritting contact and the extent of electrode damage.[34,35] To minimize damage to the superconducting film, we selected a contact force of 10 μN for testing, which is significantly lower than the mechanical breakdown contact force of 30 mN–100 mN. Figure 1(c) shows the variations in voltage and current during a typical fritting contact. As the applied voltage gradually increases, naturally oxidized aluminum is electrically broken

down, which results in a transient current in the circuit. Subsequently, the current limiter activates, rapidly reducing the current to 10 μA. This method allows us to identify the threshold fritting voltage and control the heat at the contact point, preventing damage to the aluminum film. Figure 1(d) illustrates that the contact resistance decreases as the limiting current increases. This is due to thermal expansion at the contact point caused by the heat from the higher current, which increases the contact area and consequently decreases the contact resistance. At a limiting current of 100 mA, the contact resistance is minimized to within 1 Ω. To protect the Josephson junction barrier, we set the limiting current to 10 μA, and the higher contact resistance is eliminated by using the four-terminal measurement method.

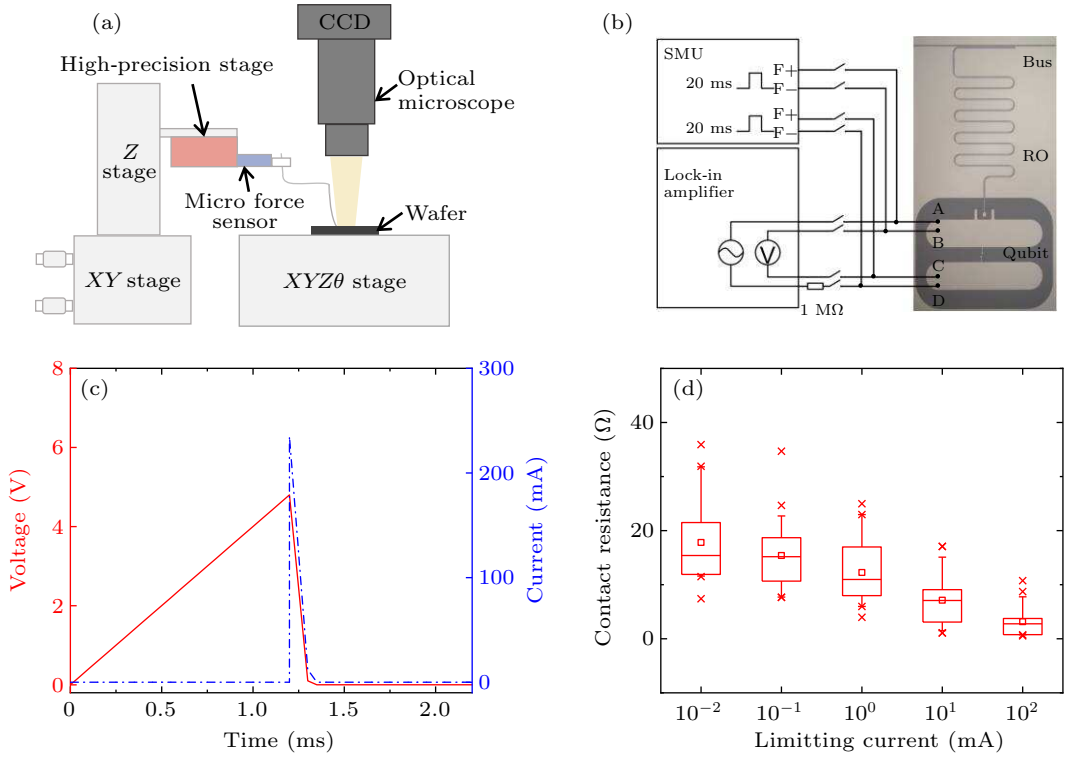


Fig. 1. Schematic of the probe measurement device and measurement setup. (a) The stage moves the chip to the measurement position with a precision of 200 nm. The probe holder moves the probe over a wide range with a precision of 1 μm. The piezoelectric stage moves the probe in the z-direction with a precision of 1 nm. The microforce sensor utilizes a cantilever structure to measure the applied force by monitoring the degree of bending in the beam under load. This bending induces a charge in the piezoelectric material within the sensor, which is then converted into an electrical signal representing the magnitude of the force. In our experiments, we monitored the contact force at the probe tip at a frequency of 50 Hz. The microscope, positioned diagonally above the sample stage, observes the probe and chip structures. (b) Schematic of the fritting and R_n measurement. Probe contacts with the qubit capacitor are labeled A, B, C, and D. The source measure unit (SMU) provides fritting pulse signals with a pulse width of 20 ms, using output terminals F+ and F–. The lock-in amplifier measures resistance using the four-terminal method. It applies a 0.1 V, 1 kHz sine wave signal across terminals A and D, while measuring the voltage across terminals B and C. The right side shows an optical image of the transmon, where the qubit capacitor is coupled to a quarter-wavelength coplanar waveguide resonator (RO) and controlled via a bus (BUS). (c) Typical time-dependent behavior of fritting contact, showing the variation of fritting voltage and current over time. In the figure, the fritting voltage is 4.8 V, with a current limit of 10 μA. (d) Relationship between limiting current and contact resistance. Each box plot represents the mean (square), median (line within the box), 10%–90% values (whiskers), interquartile range (box boundaries), and outliers (crosses).

To determine the precision of predicting f_q using the fritting contact method, we measured R_n of 24 qubits at room temperature and compared the results with the corresponding f_q measured at low temperature. The qubits underwent R_n measurement, packaging, and installation into a dilution refrigerator within five hours to minimize the impact of aging and drift on R_n. Here f_q is referred to as the bare frequency of qubit, which was first measured using the Ramsey fringe method and was then downshifted by an amount of dispersive shift to rule out the dressing effect arising from the coupling to readout resonator.[36] Figure 2 shows the relationship between f_q and R_n, which fits well with a power-law relationship, as expected from transmon theory. The inset in Fig. 2 shows that the residuals between f_q and the fitted curve follow a Gaussian distribution with a standard deviation of 17.2 MHz, indicating that we can predict f_q with an error of 17.2 MHz using the power-law relationship and R_n measured by the fritting contact method. This level of precision is comparable to the state-of-the-art frequency prediction error of 14.5 MHz demonstrated by IBM on fixed-frequency qubit.[16] In our case, this error mainly comes from the uncertainty of qubit capacitance due to variations in the fabrication process, while fluctuation in the superconducting gap also contributes. We observed a slight deviation between the power-law fitting exponent (−0.48) and

the theoretical value (-0.5), which can be attributed to the fact that R_n is measured at room temperature rather than the cryogenic value used in the theory.

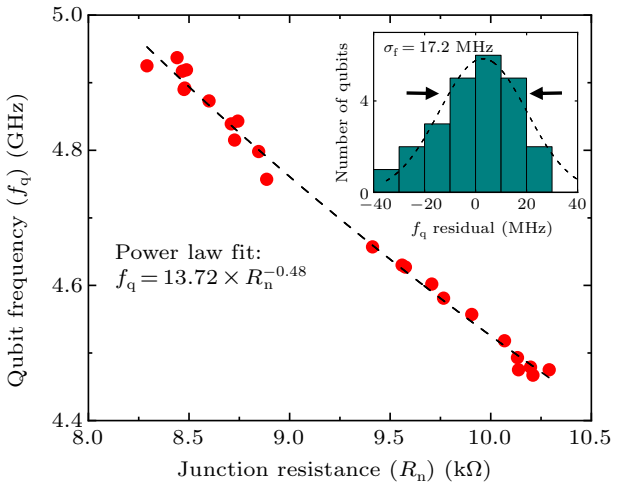


Fig. 2. Plot showing the relationship between f_q and R_n, along with the power-law fitting curve. The inset presents the statistical distribution of the residuals of f_q from the fitted values. To account for the dressing effect due to the coupling between qubit and its readout resonator, the qubit frequency f_q measured using the Ramsey fringe method was downshifted by dispersive shift $\chi = g^2/\delta$, where g and δ are the coupling strength and frequency detuning between qubit and its readout resonator. In our case, $g \approx 80$ MHz, $\delta \approx 2$ GHz, which gives $\chi \approx 3.2$ MHz.

In addition to precise frequency prediction, maintaining high qubit performance is also crucial. We investigated the impact of fritting contact on qubit coherence and the aluminum film. Qubit coherence is a critical parameter for high-fidelity gate operations and is highly sensitive to dielectric loss in materials.[37,38] We analyzed the distribution of energy relaxation time (T_1) and phase relaxation time (T_2) for 24 qubits before and after R_n measurement, as shown in Fig. 3(a). In the quantile–quantile plot (left panel), T_1 and T_2 exhibit a good correspondence with the unit slope, indicating that qubit coherence has a similar distribution before and after R_n measurement. The box plots (right panel) provide a detailed comparison of the means, quantiles, and other distributions of T_1 and T_2. Before (after) resistance measurement, T_1 is 42 ± 14 μs (43 ± 14 μs), and T_2 is 24 ± 13 μs (22 ± 11 μs), demonstrating that fritting contact did not affect qubit coherence within the statistical error range. Figure 3(b) shows the morphology of the aluminum film when mechanical breakdown of the oxide layer is used to achieve electrical contact between the probe and the electrode. Such indentations may affect capacitance C_q and introduce impurities, which reduce coherence time. We compared the morphology at the contact point before and after fritting contact and found no indentations, as shown in Figs. 3(c) and 3(d). This is achieved by precisely controlling the breakdown voltage and contact force, while the active vibration isolation table effectively isolates environmental noise. Overall, these results indicate that fritting contact is non-destructive for superconducting qubits.

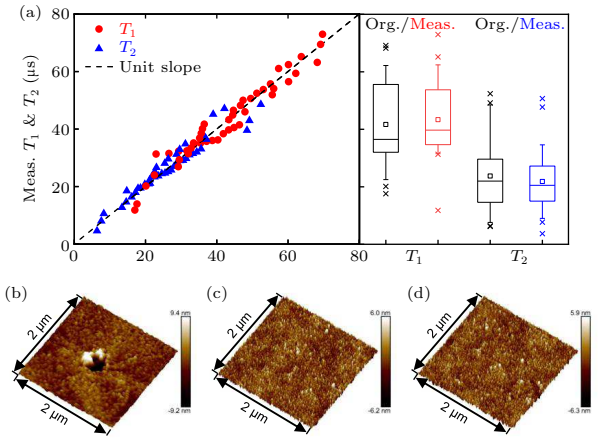


Fig. 3. (a) The effect of fritting contact on qubit coherence. The left panel presents a quantile–quantile (QQ) plot comparing data before and after resistance measurement. The right panel is a box plot showing the mean (square), median (line within the box), 10%–90% range (whiskers), interquartile range (box boundaries), and outliers (crosses). "Org." stands for original, and "Meas." stands for measured, corresponding to the values before and after resistance measurement, respectively. (b)–(d) AFM measurements of the surface morphology at the contact points on the aluminum film. Panel (b) illustrates the mechanical breakdown of the oxide layer, panel (c) shows the surface before fritting contact, and panel (d) shows the surface after fritting contact.

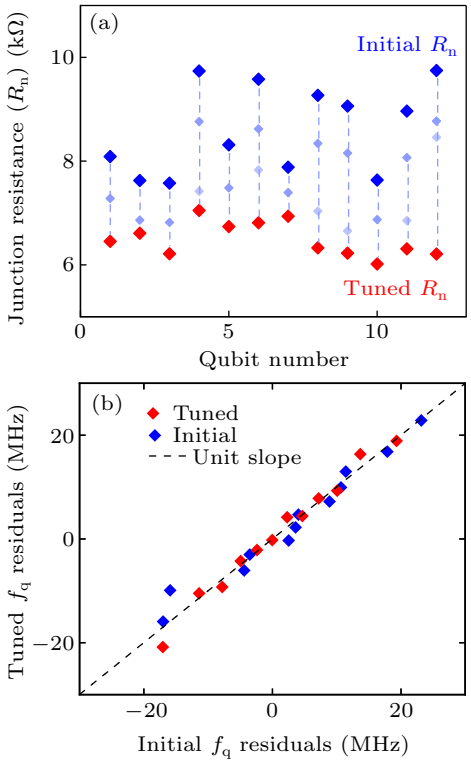


Fig. 4. (a) Resistance changes of Josephson junctions in 12 qubits during laser annealing. The blue diamonds represent the initial resistance, the light blue diamonds represent the resistance after a single laser annealing, and the red diamonds represent the final resistance. (b) Quantile–Quantile (QQ) plot of the residuals between the qubit frequencies and the fitted curve, using the same fitting curve before and after laser annealing.

Laser annealing for frequency tuning requires multiple R_n measurements to ensure tuning accuracy.[16] This demands that R_n measurement is robust. To study the impact of fritting contact on frequency tuning, we collected the parameters of

12 qubits before and after laser annealing. Figure 4(a) shows the variation of R_n with laser annealing, where each qubit undergoes multiple R_n measurements to reach its target value. Figure 4(b) presents the residual distribution between f_q and the fitted curve (using the same statistical method as the inset of Fig. 2). The residual values before and after annealing align well with a unit slope, indicating that fritting contact is well suited for frequency tuning technologies such as thermal annealing and laser annealing.

4. Conclusion

In conclusion, we have developed a novel measurement technique utilizing the fritting contact method to achieve *in situ*, non-destructive measurements of Josephson junction resistance. This technique overcomes the limitations of traditional four-probe methods, which can damage superconducting thin films and lead to inaccurate measurements. Our results show that the fritting contact method allows for precise prediction of qubit frequency with a margin of error of 17.2 MHz. Additionally, the technique does not significantly impact qubit coherence time or the integrity of the superconducting film, confirming its non-destructive nature.

The successful implementation of this method provides a robust technological foundation for precise frequency tuning, essential for mitigating frequency collision issues in multi-qubit systems. This advancement is crucial for the continued development and scalability of superconducting quantum computing. Future work will focus on further refining this technique and exploring its application in various superconducting quantum computing architectures to enhance performance and reliability.

Acknowledgments

Project supported by the National Natural Science Foundation of China (Grant Nos. 12034018 and 11625419). This work was partially carried out at the USTC Center for Micro and Nanoscale Research and Fabrication.

References

[1] He K Y, Geng X, Huang R T, *et al.* 2021 *Chin. Phys. B* **30** 080304
[2] Zheng W and Yu Y 2023 *Physics* **52** 731
[3] Brecht T, Pfaff W, Wang C, *et al.* 2016 *npj Quantum Information* **2** 16002
[4] Rosenberg D, Kim D, Das R, *et al.* 2017 *npj Quantum Information* **3** 42
[5] Walter T, Kurpiers P, Gasparinetti S, *et al.* 2017 *Phys. Rev. Appl.* **7** 054020
[6] Bultink C C, Tarasinski B, Haandbæk N, *et al.* 2018 *Appl. Phys. Lett.* **112** 092601
[7] Richardson C J K, Lordi V, Misra S, *et al.* 2020 *MRS Bulletin* **45** 485
[8] Burnett J J, Bengtsson A, Scigliuzzo M, *et al.* 2019 *npj Quantum Information* **5** 54
[9] Ware M, Johnson B R, Gambetta J M, *et al.* 2019 arXiv:1905.11480
[10] Brink M, Chow J M, Hertzberg J, *et al.* 2018 2018 *IEEE International Electron Devices Meeting (IEDM),* December 1–5, 2018, San Francisco, CA, USA, p. 6.1.1
[11] Chow J M, Córcoles A D, Gambetta J M, *et al.* 2011 *Phys. Rev. Lett.* **107** 080502
[12] Osman A, Fernández-Pendás J, Warren C, *et al.* 2023 *Phys. Rev. Res.* **5** 043001
[13] Kreikebaum J M, O'Brien K P, Morvan A, *et al.* 2020 *Supercond. Sci. Technol.* **33** 06LT02
[14] Moskaleva D A, Korshakov N D, Moskalev D O, *et al.* 2024 arXiv: 2403.01894
[15] Takahashi T, Kouma N, Doi Y, *et al.* 2022 *Jpn. J. Appl. Phys.* **62** SC1002
[16] Hertzberg J B, Zhang E J, Rosenblatt S, *et al.* 2021 *npj Quantum Information* **7** 129
[17] Zhang E J, Srinivasan S, Sundaresan N, *et al.* 2022 *Sci. Adv.* **8** eabi6690
[18] Kim H, Jünger C, Morvan A, *et al.* 2022 *Appl. Phys. Lett.* **121** 142601
[19] Koch J, Yu T M, Gambetta J, *et al.* 2007 *Phys. Rev. A* **76** 042319
[20] Wu X, Long J L, Ku H S, *et al.* 2017 *Appl. Phys. Lett.* **111** 032602
[21] Costache M V, Bridoux G, Neumann I, *et al.* 2012 *J. Vac. Sci. Technol.* **30** 04E105
[22] Foroozani N, Hobbs C, Hung C C, *et al.* 2019 *Quantum Sci. Technol.* **4** 025012
[23] Ambegaokar V and Baratoff A 1963 *Phys. Rev. Lett.* **10** 486
[24] Liu D S, Shih M K and Huang W H 2007 *Microelectronics Reliability* **47** 1086
[25] Wang C, Li X, Xu H, *et al.* 2022 *npj Quantum Information* **8** 3
[26] Kwon S, Fadavi Roudsari A, Benningshof O W B, *et al.* 2018 *J. Appl. Phys.* **124** 033903
[27] Ye Y, Ge Z Y, Wu Y, *et al.* 2019 *Phys. Rev. Lett.* **123** 050502
[28] Wang Z, Li H, Feng W, *et al.* 2020 *Phys. Rev. Lett.* **124** 013601
[29] Zhong Y, Chang H S, Bienfait A, *et al.* 2021 *Nature* **590** 571
[30] Arute F, Arya K, Babbush R, *et al.* 2019 *Nature* **574** 505
[31] Kataoka K, Itoh T, Inoue K, *et al.* 2004 *17th IEEE International Conference on Micro Electro Mechanical Systems*
[32] Kataoka K, Kawamura S, Itoh T, *et al.* 2003 *Sensors and Actuators A: Physical* **103** 116
[33] Itoh T, Kataoka K, Engelmann G, *et al.* 2000 *Design, Test, Integration, and Packaging of MEMS/MOEMS* **4019** 244
[34] Kataoka K, Itoh T and Suga T 2005 *Proceedings of the Fifty-First IEEE Holm Conference on Electrical Contacts,* 2005, 2005, Chicago, IL, USA, p. 259
[35] Kataoka K, Itoh T and Suga T 2003 *IEEE Transactions on Components and Packaging Technologies* **26** 382
[36] Blais A, Huang R S, Wallraff A, *et al.* 2004 *Phys. Rev. A* **69** 062320
[37] Murray C E 2021 *Materials Science and Engineering: R: Reports* **146** 100646
[38] Lisenfeld J, Bilmes A, Megrant A, *et al.* 2019 *npj Quantum Information* **5** 105